CHEMISTRY
AN ASIAN JOURNAL

DOI: 10.1002/asia.201100972

Naphthyl and Thienyl Units as Bridges for Metal-Free Dye-Sensitized Solar Cells

Yung-Chung Chen,[a] Yo-Hua Chen,[b] Hsien-Hsin Chou,[a] Sumit Chaurasia,[a] Yuh S. Wen,[a] Jiann T. Lin,*[a] and Ching-Fa Yao*[b]

Abstract: A series of new organic dyes, comprising a naphthyl moiety as a π-conjugated bridge, different amines as donors, and a cyanoacrylic acid group as an electron acceptor and anchoring group, have been designed and synthesized for applications in dye-sensitized solar cells (DSSCs). One of the compounds was also characterized by single-crystal X-ray structural analysis. All of the dyes exhibited maximum absorptions in the range of 371–441 nm. The short-circuit photocurrent density, open-circuit voltage, and fill factor (*FF*) values of the devices are in the range of 6.13–10.90 mA cm^{-2}, 0.62–0.69 V, and 0.62–0.67, respectively, corresponding to an overall conversion efficiency of 2.76–4.55 %. The conversion efficiency reached 38–62 % of that of a N719-based device (7.31 %) fabricated and measured under similar conditions. Steric congestion between the naphthyl and aromatic moieties jeopardizes charge transfer from the donor to the acceptor. Insertion of an alkenyl entity between the naphthyl entity and the aromatic ring alleviates steric congestion and leads to longer wavelength electronic absorption spectra.

Keywords: donor–acceptor systems · dyes/pigments · solar cells · sensitizers

Introduction

Since the seminal report by O'Regan and Grätzel in 1991,[1] dye-sensitized solar cells (DSSCs) have received extensive interest because of their low cost and relatively high solar energy to electricity conversion efficiency (η).[2] The efficiencies of DSSCs are affected by various factors of the sensitizers, such as molecular structure, photophysical, and electrochemical properties.[2,3] So far, ruthenium(II) polypyridyl complexes still stand out as the most efficient and stable sensitizers for DSSCs and the record high conversion efficiency is ≧11 %.[4] Moreover, ruthenium-based dyes usually exhibit higher open-circuit voltages (V_{OC}) than metal-free sensitizers. However, the expense and toxicity of these materials may limit their applications in DSSCs.

Compared with ruthenium(II) polypyridyl complex based dyes, metal-free organic dyes possess larger molar extinction coefficients and facile structure modification, therefore, they are attracting more and more research efforts. Various organic dyes with acceptable stability and high cell efficiency have been obtained in recent years.[5] A record efficiency of up to 10 % has been achieved for metal-free DSSCs.[6] Excellent temporal stability with a durable efficiency of 7–8 % at 60 °C for at least 1000 h was also demonstrated for organic dyes.[7]

Sensitizers with higher molar extinction coefficients and longer absorption wavelengths are advantageous for high cell efficiency. In our studies on metal-free dyes for DSSCs applications, we have developed a series of arylamine-based compounds with various heteroaromatic rings in the conjugated spacers and achieved high-performance DSSCs by using these dyes as sensitizers.[8] A common feature of these molecules is the high intensity of their electronic absorption. Heteroaromatic rings in these compounds should also play an important role because of their higher tendency than the phenyl entity to form a quinoid structure during charge-transfer transitions. Conversion of the aromatic unit in the conjugated chain into a quinoid structure will lead to a small band gap, however, at the expense of stability due to destruction of the aromaticity.[9] A more favorable quinoid structure is therefore anticipated upon replacement of a phen-1,4-diyl unit with naphtha-1,4-diyl or anthracen-9,10-diyl units. Indeed, Pugh et al. observed a bathochromic shift of the absorption wavelength in azoarenes when the phen-1,4-diyl unit in the spacer was replaced by a naphtha-1,4-diyl unit.[10] Anthracene-bridged metal-free sensitizers developed by Sun et al. had high efficiencies of up to 7.03 % despite the large dihedral angle between the anthracenyl unit and the neighboring phenyl ring.[11] Although the naphthyl-bridged zinc porphyrin carboxylic acid investigated by Ima-

[a] Dr. Y.-C. Chen, Dr. H.-H. Chou, Dr. S. Chaurasia, Y. S. Wen, Prof. Dr. J. T. Lin
Institute of Chemistry
Academia Sinica
11529, Nankang, Taipei (Taiwan)
Fax: (+886) 783-1237
E-mail: jtlin@chem.sinica.edu.tw

[b] Y.-H. Chen, Prof. Dr. C.-F. Yao
Department of Chemistry
National Taiwan Normal University
117, Taipei (Taiwan)
E-mail: cheyaocfh@ntnu.edu.tw

Supporting information for this article is available on the WWW under http://dx.doi.org/10.1002/asia.201100972.

hori et al. indicated the existence of a large dihedral angle between the naphthyl unit and the porphyrin ring,[12] the steric constraint between naphtha-1,4-diyl and phen-1,4-diyl units should be somewhat released compared with that between a anthracen-9,10-diyl unit and a phen-1,4-diyl unit. Moreover, appropriate deviation of a sensitizer molecule from planarity could avoid dye aggregation and/or close contact of electrolyte molecules with the TiO_2 surface. Therefore, we turned our attention to metal-free dyes containing naphtha-1,4-diyl units in the conjugated bridge. Herein, we report new metal-free dyes containing one or more naphtha-1,4-diyl units in the conjugated bridge. Their photophysical properties and the performance of the DSSCs fabricated are also discussed.

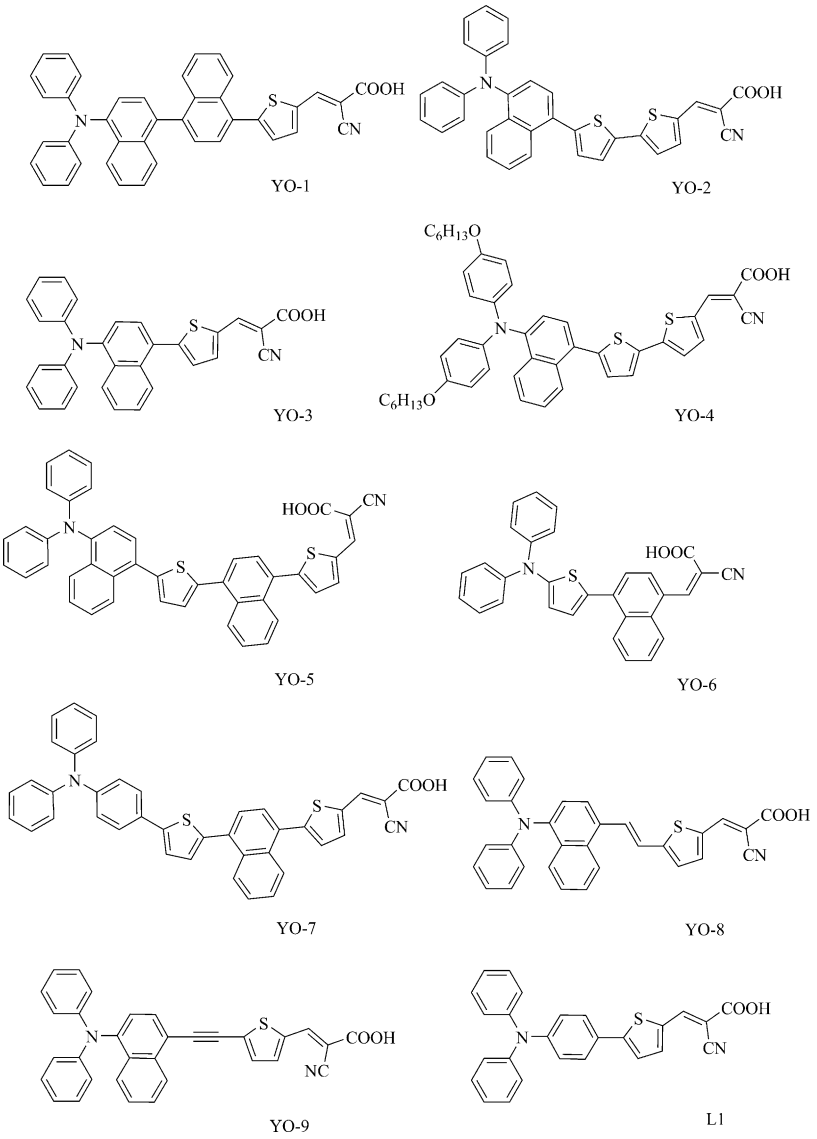

Scheme 1. Structures of compounds YO1–YO9 and reference compound L1.

Results and Discussion

Synthesis and Characterization

The structures of new metal-free sensitizers are shown in Scheme 1. The synthetic protocols for compounds YO-1 to YO-5 and YO-6 to YO-9 are illustrated in Schemes 2 and 3, respectively. The following key steps are involved in the synthetic protocols: 1) a palladium-catalyzed Buchwald–Hartwig C–N coupling reaction for incorporation of arylamine (steps i and ii in Scheme 2 and step v in Scheme 3);[13] 2) a palladium-catalyzed Stille coupling reaction between a stannyl compound and an aryl bromide (steps iii, vii, ix, and x in Scheme 2, and step i in Scheme 3);[14] 3) formylation of the heteroaromatic ring (step iv in Scheme 2, and steps iii and vi in Scheme 3); 4) a Sonogashira coupling reaction between arylamine and thiophene bromide (step ix in Scheme 3);[15] 5) condensation of an aromatic aldehyde with cyanoacetic acid with the formation of 2-cyanoacrylic acid (step v in Scheme 2 and step ii in Scheme 3). The dyes are obtained as yellow to dark red powders and are soluble in common organic solvents, such as tetrahydrofuran (THF), CH_2Cl_2, and $CHCl_3$. The structure of YO-8 was also confirmed by single-crystal X-ray diffraction analysis and the ORTEP plot is shown in Figure 1. Important bond lengths, bond angles, and dihedral angles of the molecule are compiled in Table S1 in the Supporting Information and more details are shown in Figure S1. Although the thiophene ring is nearly coplanar with the two neighboring vinyl entities, there is significant deviation of the naphthyl unit from coplanarity with the neighboring vinyl entity (dihedral angle = 34.05°). The carboxylic group and the thiophenyl ring are in mutual *trans*

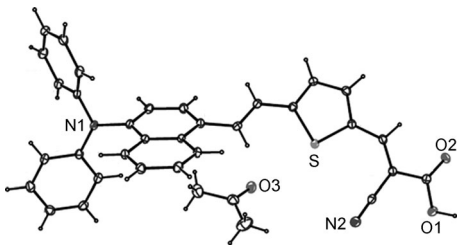

Figure 1. ORTEP diagram of YO-8 with thermal ellipsoids shown at the 30% probability level.

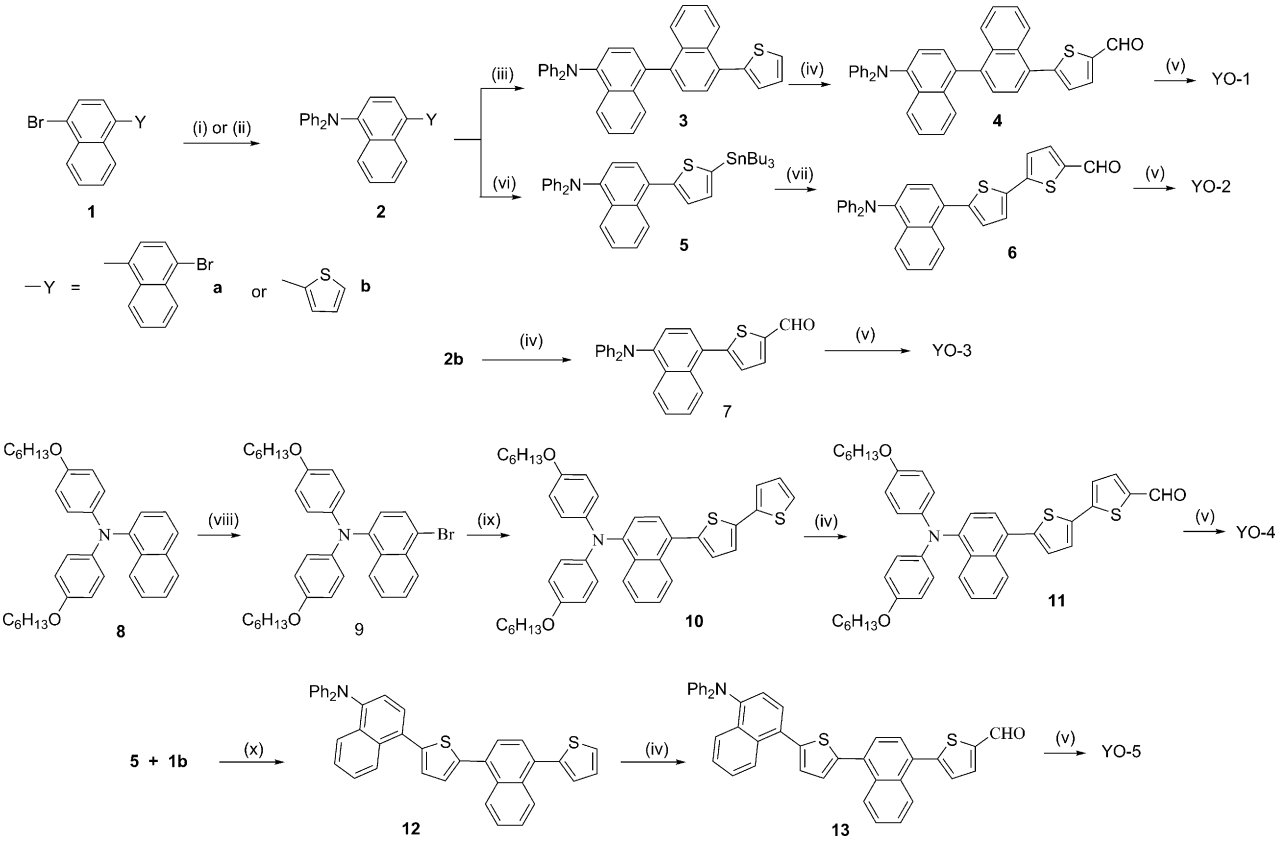

Scheme 2. Synthesis of YO1–YO5.[a] Reagents and conditions: i) Ph_2NH, *t*BuONa, $[Pd(dba)_2]$ (dba = dibenzylideneacetone), 1,1′-bis(diphenylphosphino)-ferrocene (dppf); ii) Ph_2NH, *t*BuONa, $Pd(OAc)_2$, P*t*Bu_3; iii) tributylthiophen-2-ylstannane, $[Pd(PPh_3)_2Cl_2]$; iv) a) *n*BuLi, b) *N*,*N*-dimethylformamide (DMF), c) 2 N HCl; v) cyanoacetic acid, NH_4OAc, acetic acid; vi) a) *n*BuLi, b) Bu_3SnCl; vii) 5-bromothiophene-2-carbaldehyde, $[Pd(PPh_3)_4]$; viii) *N*-bromosuccinimide (NBS); ix) 2,2′-bithiophenyl-5-yltributylstannane, $[Pd(PPh_3)_4]$; x) $[Pd(PPh_3)_4]$.

positions of the vinyl group. Compared with the *cis* isomer, such a conformation may avoid charge trapping at the cyano moiety and facilitate electron injection into TiO_2.

Photophysical Properties

The absorption spectra of the new dyes in THF are shown in Figure 2a and the data are summarized in Table 1. The absorption band at a shorter wavelength is attributed to a localized π–π* transition. The broad band at a longer wavelength, ranging from 371 to 441 nm, is due to charge transfer mixed with a more delocalized π–π* transition. Taking YO-3 as an example, the charge-transfer character of the band is evidenced from the following observations: replacement of the 2-cyanoacrylic acid moiety in YO-3 by a formyl group (**7** in Scheme 2) and a hydrogen atom (**2b** in Scheme 2) leads to a decrease in λ_{max} by 30 (417 vs. 387 nm in THF) and 51 nm (417 vs. 366 nm in THF), respectively.

Table 1. Electro-optical parameters of the dyes.

Dyes	λ_{abs} [nm] ($\varepsilon\times10^{-4}$ [M^{-1} cm^{-1}])[a]	λ_{em}[a] [nm]	$E_{1/2}$ (ox)[b] [mV]	HOMO/LUMO [eV]	$E_{0\text{-}0}$[c] [eV]	$E_{0\text{-}0^*}$[d] [eV]
YO-1	379 (3.22), 293 (3.17)	529	577 (85)	5.38/2.52	2.86	−1.48
YO-2	428 (3.99), 276 (9.10)	625	536 (73), 833 (86)	5.34/2.71	2.63	−1.28
YO-3	414 (1.36), 356 (1.67), 277 (10.6)	607	585 (88)	5.39/2.99	2.40	−1.01
YO-4	422 (2.56), 276 (7.43)	589	250 (91), 850 (86)	5.05/2.54	2.51	−1.46
YO-5	382 (2.80), 277 (6.05)	539	522 (79), 797 (86)	5.32/2.56	2.76	−1.44
YO-6	401 (1.04), 273 (5.29)	568	389 (78)	5.19/2.79	2.40	−1.21
YO-7	371 (3.64), 277 (9.28)	527	421 (86), 832 (86)	5.22/2.54	2.68	−1.46
YO-8	441 (3.89), 294 (3.37)	567	499 (66)	5.30/3.02	2.28	−0.98
YO-9	414 (2.86), 370 (2.45), 292 (2.31)	538	603 (125)	5.40/3.01	2.39	−0.99

[a] Recorded in THF. [b] Recorded in CH_2Cl_2; scan rate = 100 $mV\,s^{-1}$; electrolyte = $(n\text{-}C_4H_9)_4NPF_6$; potentials are quoted with reference to the internal ferrocene standard ($E_{1/2}$ = +50 mV vs. $Ag/AgNO_3$). [c] The band gap, $E_{0\text{-}0}$, was derived from the intersection of the absorption and emission spectra. [d] $E_{0\text{-}0^*}$: the excited-state oxidation potential versus a normal hydrogen electrode (NHE).

The absorption wavelength of the compounds decreases in the order of YO-8 > YO-2 > YO-4 > YO-9 > YO-3 > YO-6 > YO-5 > YO-1 > YO-7. The large dihedral angle (see below) between the naphthyl and neighboring aromatic ring will jeopardize charge transfer. Therefore, it is not surprising that YO-1 has a very small λ_{max} value owing to the presence of two sterically congested naphthyl entities. In comparison, compound YO-8 has a longer λ_{max} value than the others

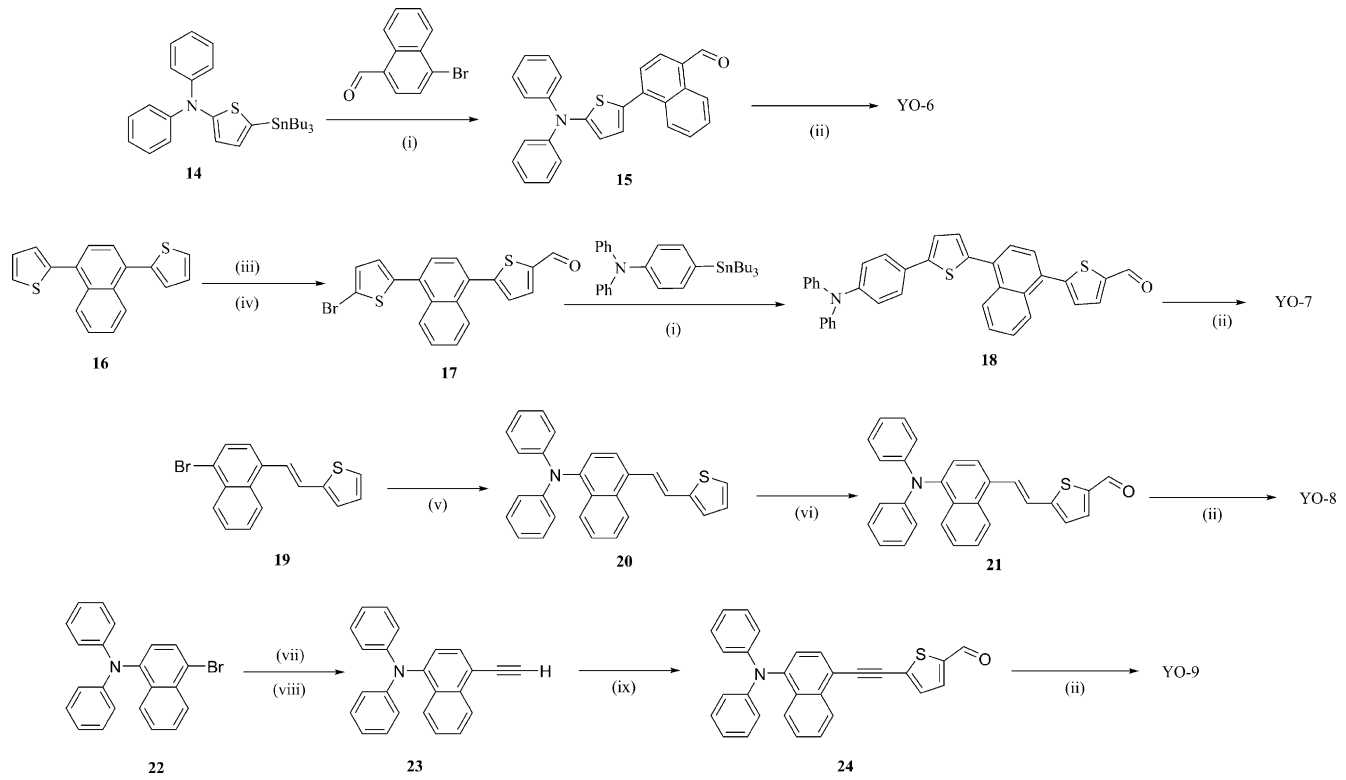

Scheme 3. Synthesis of YO6–YO9.[a] Reagents and conditions: i) $[Pd(PPh_3)_4]$; ii) cyanoacetic acid, NH_4OAc, acetic acid; iii) a) *n*BuLi, b) DMF, c) 2 N HCl; iv) NBS; v) Ph_2NH, *t*BuONa, $Pd(OAc)_2$, P*t*Bu$_3$; vi) $POCl_3$, DMF; vii) trimethylsilylacetylene, CuI, *i*Pr$_2$NH, $[PdCl_2(PPh_3)_2]$, tetrahydrofuran (THF); viii) KF, MeOH; ix) 5-bromo-2-thiophenecarbaldehyde, CuI, *i*Pr$_2$NH, $[PdCl_2(PPh_3)_2]$.

owing to better coplanarity (see below) of the molecule. Compound YO-9 absorbs at a shorter wavelength (λ_{max} = 414 nm) than that of YO-8 (λ_{max} = 441 nm), even though the conjugated spacer of the former is much more planar than that of the latter (see below). This can be attributed to the poorer orbital match of the aromatic p orbital (naphthyl and thienyl entities) with the alkynyl p orbital in energy.[16] Compounds with the longest conjugated spacer between the donor and the acceptor, YO-5 and YO-7, have short absorptions, most likely the severe twist of the aromatic rings from coplanarity hampers effective electronic delocalization and charge transfer; however, saturation of conjugation in these compounds cannot be ruled out. Elongation of the effective conjugation length results in a redshift of the absorption spectrum: λ_{max} (YO-2) > λ_{max} (YO-3). Compared with YO-2, the absorption maximum of YO-4 is slightly blueshifted; however, the long wavelength tailing of the latter is redshifted, which is in agreement with the better donating power of arylamine upon incorporation of alkoxy units at the phenyl rings.

One aim of this work was to study the possibility of quinoid structure of the naphthyl moiety in the spacer resulting in a redshift of the electronic absorption. Compound YO-3 was therefore selected for comparison with its congener, L1 (Scheme 1),[17] in which the naphthyl unit in YO-3 was replaced with a phenyl-1,4-diyl entity. Compound YO-3 has a blueshifted absorption with a lower intensity than that of L1 (444 nm, ε = 27490 $M^{-1}cm^{-1}$). Apparently the nonplanar conformation of the spacer blocks YO-3 from forming a quinoid structure. A redshift of the longer wavelength tail from YO-5 to YO-7 may also be attributed to impediment of the quinoid structure owing to the more twisted conformation in the former. A significant blueshift of the spectra of the dyes on TiO_2 surfaces (see Figure S2 in the Supporting Information) may be caused by deprotonation of the carboxylic acid;[8d] this was also confirmed by measuring the absorption of the dyes in the presence of Et_3N. A certain degree of J aggregation[18] may also occur, as evidenced from the prominent red tailing of the absorption spectra.

The λ_{max} value of the charge-transfer band in YO-2 decreases as the solvent polarity increases, that is, toluene (444) > 1,4-dioxane (440) > THF (437) > acetone (415) ≈ MeOH (415) > DMF (407 nm) (see Figure S3 in the Supporting Information). Negative solvatochromism may be attributed to the strong interaction of polar solvent with the dyes, which weakens the O–H bond of the carboxylic acid and consequently decreases the electron-withdrawing nature of the COOH group.[19] The compounds are weakly emissive in the green to red region (Figure 2b); luminescence data are presented in Table 1. It was noted that YO-1, YO-2, and YO-7 had structured emission spectra. Therefore, excitation spectra were measured for YO-2 (Figure 3). The excitation spectrum obtained upon monitoring at 480 nm (the blue side in the emission spectrum) was different from that ob-

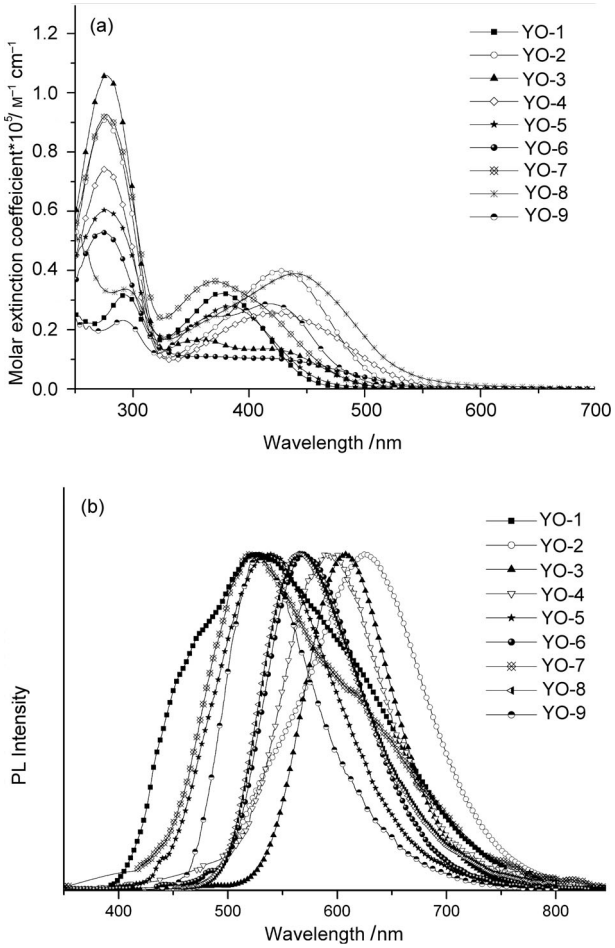

Figure 2. a) UV/Vis and b) photoluminescence (PL) spectra of YO-1–YO-9 recorded in THF.

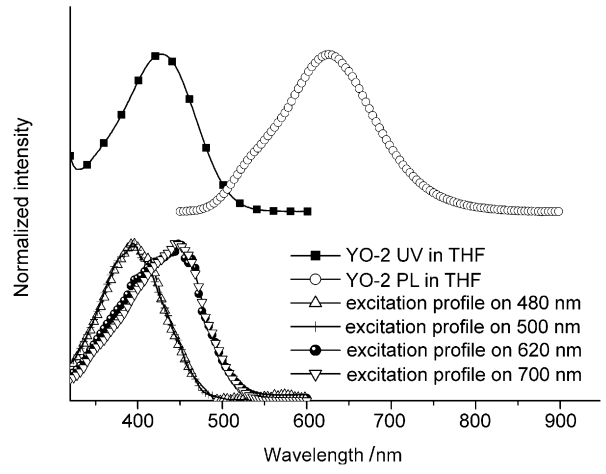

Figure 3. Absorption and emission spectra and excitation profiles of YO-2 in THF.

tained from monitoring at 700 nm (the red side of the emission spectrum). The dual emission may be due to the presence of different excited structures owing to the restricted rotation of the naphthyl entity.

Electrochemical Properties

The electrochemical properties of the dyes were studied by cyclic voltammetry (CV) and differential pulse voltammetry (DPV). The relevant CV data are collected in Table 1 and selected cyclic voltammograms are shown in Figure 4. Only one quasi-reversible redox wave was observed for YO-1, YO-3, YO-6, YO-8, and YO-9 owing to oxidation of the arylamine. In addition to the first redox wave stemming from oxidation of the arylamine, other compounds exhibited a second quasi-reversible redox wave, most likely from oxidation of the conjugated segment because of the presence of two electron-rich thiophene rings. The first oxidation potential of the compounds decreases in the order of YO-9 > YO-3 > YO-1 > YO-2 > YO-5 > YO-8 > YO-7 > YO-6 > YO-4.

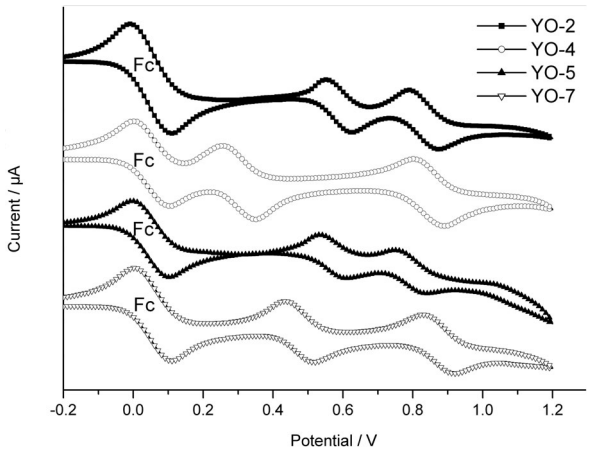

Figure 4. Cyclic voltammograms of YO-2, YO-4, YO-5, and YO-7 recorded in CH_2Cl_2.

The lower oxidation potential of YO-4 than YO-2 can be attributed to the presence of an electron-donating alkoxy group at the phenyl ring, when compared with similar compounds reported in the literature.[20] As expected, compound YO-6 was oxidized at a lower potential because of the direct linkage of a thienyl moiety with the nitrogen atom of arylamine.[21] Compound YO-7 has a lower oxidation potential than that of YO-5. The smaller dihedral angle (see below) of the phenyl/thienyl segment than the naphthyl/thienyl segment is likely to lead to a more stabilized cationic arylamine as a result of better electronic interaction between the arylamine and the thiophene ring. The energy levels of the HOMOs of these materials were calculated with reference to ferrocene (4.8 eV) and ranged from 5.05 to 5.40 eV. This together with the HOMO/LUMO gap ($E_{0\text{-}0}$, 2.28–2.86 eV) obtained from the intersection of the absorption and emission spectra was utilized to derive the LUMO energy. The excited-state oxidation potentials ($E_{0\text{-}0}$*) of the sensitizers, estimated from the difference between the first oxidation potential at the ground state and $E_{0\text{-}0}$, are more negative (−0.98 to −1.48 V vs. NHE; see Table 1) than the conduction band edge of TiO_2 (−0.5 V vs. NHE).[22] Therefore,

electron injection from the excited dye to TiO_2 should be energetically favorable. Dye regeneration by the electrolyte is also expected to be favorable because the first oxidation potentials of the dyes are more positive (1.39–1.05 V vs. NHE) than that of the I^-/I_3^- redox couple (0.4 V vs. NHE).[23]

Photovoltaic Properties

DSSCs were fabricated with the use of the new dyes and nanocrystalline anatase TiO_2. The cells had an effective area of 0.25 cm^2 and the electrolyte used was composed of 0.05 M I_2/0.5 M LiI/0.5 M *tert*-butylpyridine (TBP) in acetonitrile. The device performance statistics under standard global illumination from one sun (AM 1.5) are presented in Table 2. A

Table 2. Photovoltaic properties of the cells.[a]

Dyes	V_{oc} [V]	J_{SC} [mA cm^{-2}]	η [%]	*FF*	R_{ct} [Ω]
YO-1	0.68	6.13	2.76	0.66	50
YO-2	0.66	10.80	4.45	0.63	30
YO-3	0.64	7.16	3.04	0.67	50
YO-4	0.66	9.47	3.99	0.64	31
YO-5	0.67	7.49	3.26	0.65	42
YO-6	0.65	8.33	3.58	0.66	24
YO-7	0.69	9.19	3.90	0.62	24
YO-8	0.64	10.90	4.55	0.65	20
YO-9	0.62	7.97	3.30	0.67	33
L1	0.66	9.97	4.29	0.65	27
N719	0.74	15.20	7.31	0.65	18

[a] Experiments were conducted by using TiO_2 photoelectrodes approximately 18 μm thick and with a 0.25 cm^2 working area on the fluorine tin oxide (FTO) substrates.

DSSC fabricated from the aforementioned sensitizer L1[17] was also prepared for comparison. The photocurrent–voltage (*J*–*V*) curves and dark current plots are shown in Figure 5, and incident monochromatic photo-to-current conversion efficiency (IPCE) plots of the cells are shown in Figure 6. The short-circuit photocurrent density (J_{SC}), open-circuit voltage (V_{OC}), and fill factor (*FF*) values of the devices are in the range of 6.13–10.90 mA cm^{-2}, 0.62–0.69 V, and 0.62–0.67, respectively, corresponding to an overall conversion efficiency of 2.76–4.55 %. The DSSC of YO-8 has the best power conversion efficiency (4.55 %) of the compounds tested, reaching 62 % of the standard ruthenium dye N719-based cell (conversion efficiency = 7.31 %) fabricated and measured under similar conditions.

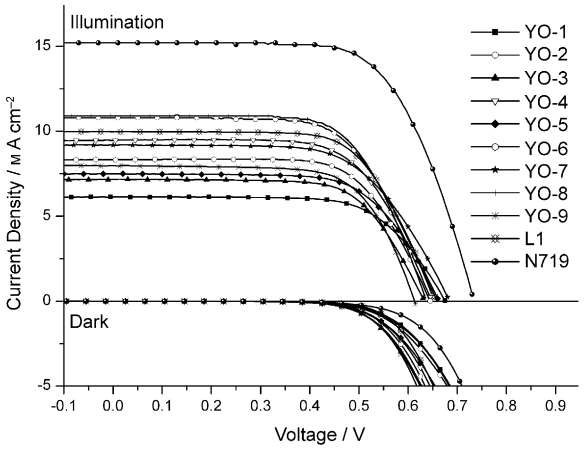

Figure 5. *J*–*V* curves and dark currents for the compounds.

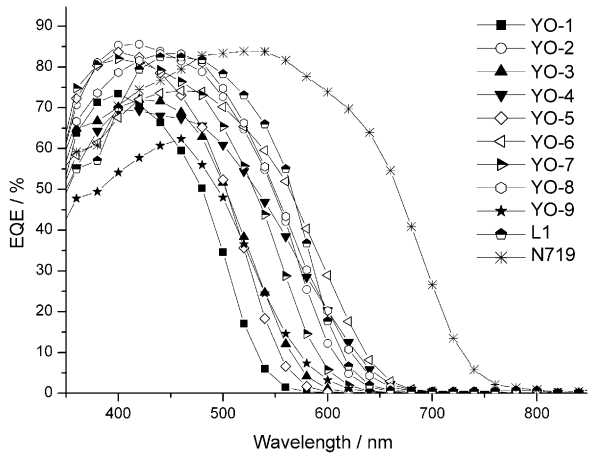

Figure 6. IPCE curves for the compounds.

The dye density on the TiO_2 film was checked and decreased in the order of YO-8 (5.08×10^{-7}) > YO-9 (4.95×10^{-7}) > YO-1 (4.68×10^{-7}) > YO-7 (4.44×10^{-7}) > YO-3 (4.30×10^{-7}) > YO-2 (4.21×10^{-7}) > YO-4 (3.65×10^{-7}) > YO-5 (3.52×10^{-7}) > YO-6 (2.59×10^{-7} mol cm^{-2}). We suspect that the higher dye density of YO-8 and YO-9 is due to the presence of the vinyl or ethynyl entity, which may decrease steric congestion of the dye molecules on TiO_2. Several factors may contribute to the higher efficiency of YO-8: 1) good light-harvesting efficiency (long absorption wavelength and high molar extinction coefficient); 2) high dye-loading density; and 3) better electron collection because of lower electron transport resistance (see below). However, the higher dark current in the devices of YO-8 led to a lower V_{OC} value and counteracted the overall efficiency. The high performance of the cell from YO-2 may also be rationalized by better light harvesting and relatively high dye-loading density. The binaphthyl entity in YO-1 seems to more effectively suppress the dark current and increases the V_{OC} value of the cell. Nevertheless, compound YO-1 has the lowest cell efficiency because of its inefficient light harvesting. The much lower cell efficiency of YO-9 than that of YO-8 can be largely attributed to the shorter absorption wavelength of the former, as evidenced from the IPCE plots. Although the dye density of L1[17] reaches only about 50 % (2.08×10^{-7} mol cm^{-2}) of that of YO-3, the cell efficiency of L1 is nearly 40 % higher than that of YO-3. Apparently light harvesting plays a very important role in cell performance. Better electron collection (see below) and dark current suppression were also found in the cell of L1.

The dark currents of all DSSCs were also measured (Figure 5) and their V_{OC} data are collected in Table 2. The V_{OC} data of DSSCs decreases in the order of N719 > YO-7 >

YO-1 > YO-5 > YO-2 ≈ YO-4 > YO-6 > YO-3 ≈ YO-8 > YO-9. Large dark currents of the cells from YO-9, YO-3, and YO-8 are consistent with their lower V_{OC} values. Electrochemical impedance measurements under illumination are shown in Figure 7. In general, electrochemical impedance

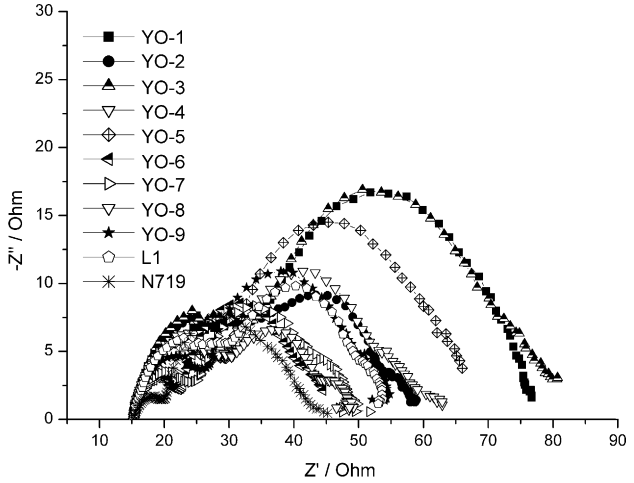

Figure 7. Electrochemical impedance spectra (Nyquist plots) of DSSCs for dyes measured under illumination (AM | 1.5).

measured under illumination provides information on electron injection and transport inside TiO_2.[24] Upon illumination with 100 mW cm^{-2} under open-circuit conditions, the radius of the intermediate frequency semicircle in the Nyquist plot (Figure 7) represents the electron transport resistance. The electron transport resistance (R_{ct}; Table 2) decreased in the order of YO-1 (50) ≈ YO-3 (50) > YO-5 (42) > YO-9 (33) > YO-4 (31) > YO-2 (30) > YO-6 (24) ≈ YO-7 (24) > YO-8 (20) > N719 (18 Ω). Lower electron transport resistance will assist electron collection and improve cell efficiency. The smallest R_{ct} value for YO-8 is consistent with it having the highest cell efficiency. In contrast, compounds YO-1 and YO-3, with higher electron transport resistance, exhibited the lowest efficiency of all of the devices. The cell of YO-3 had a larger electron transport resistance (50 Ω) than that of L1 (27 Ω), in accordance with its lower power conversion efficiency. The results obtained herein are roughly consistent with the trend observed for cell performance (Table 2).

Nyquist plots of DSSCs under a forward bias of −0.55 V in the dark are shown in Figure S4 in the Supporting Information. The second semicircle can be used to derive the charge recombination resistance on the TiO_2 surface (R_{rec}) by fitting curves using Z-view software. A larger R_{rec} value implies a smaller dark current. The R_{rec} value is roughly consistent with the trend of the dark current. Three R_{rec} values of YO-3, L1, and N719 are shown in Figure 8 for comparison. The R_{rec} value decreases in the order of N719 (760) > L1 (362) > YO-3 (186 Ω), thus suggesting that the YO-3 has more facile charge recombination. This is consistent with the lower V_{OC} value and cell efficiency of YO-3.

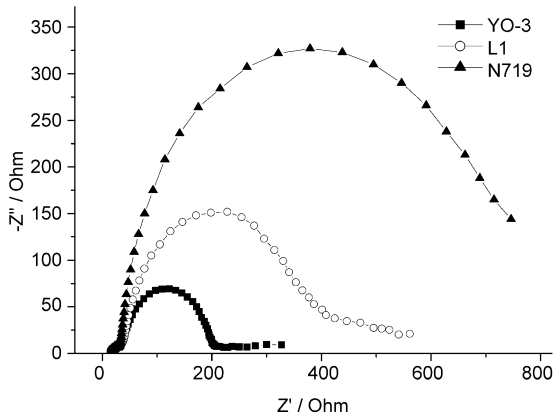

Figure 8. Electrochemical impedance spectra (Nyquist plots) of DSSC for YO-3, L1, and N719 dyes measured in the dark under −0.55 V bias.

Theoretical Approach

Quantum chemistry calculations were conducted to gain further insight into the correlation between molecular structure and physical properties as well as device performance. The computed frontier orbitals of the compounds and their corresponding energy states are included in Figures S5 and S6 in the Supporting Information, and the results for theoretical computation are listed in Table S2. The molecules were divided into several segments: the arylamine (or alkylamine) group (Am); the naphthyl, phenyl, and thiophene units (Nap, Ph, T); and the 2-cyanoacrylic acid (Ac). The Mulliken charges for the $S_0 \rightarrow S_1$ and $S_0 \rightarrow S_2$ transitions were also calculated as a projection from the time-dependent density functional theory (TD-DFT) results. Differences in the Mulliken charges in the excited and ground states were calculated and grouped into several segments in the molecules to estimate the extent of charge separation upon excitation (Figure S7 in the Supporting Information). For all compounds, the lowest energy transition ($S_0 \rightarrow S_1$, > 99 % HOMO→LUMO transition) has very prominent charge separation from arylamine to 2-cyanoacrylic acid; however, the oscillator strength (f) varies. For YO-1 and YO-5, in which the spacer is less coplanar (see below), the f values are only 0.01 and 0.10, respectively. This is consistent with the low short-circuit currents and conversion efficiencies for the two devices. Except for YO-9, compound YO-8 has the largest f value for the $S_0 \rightarrow S_1$ transition because of a more planar spacer. Moreover, the $S_0 \rightarrow S_2$ transition (mainly HOMO-1→LUMO transition) also has a large f value. A cascade transition from S_2 to S_1 will also assist electron injection. Despite of the largest f value for the $S_0 \rightarrow S_1$ transition, compound YO-9 suffers from a short absorption wavelength and less efficient dark current suppression, and therefore, results in low cell performance (see above). Although YO-4 has very similar structural features to YO-2, the former has an absorption spectrum extending to a longer wavelength. Moreover, DSSCs based on the two dyes have comparable electron transport resistances. Therefore, the inferior performance of the DSSC based on YO-4 is likely to

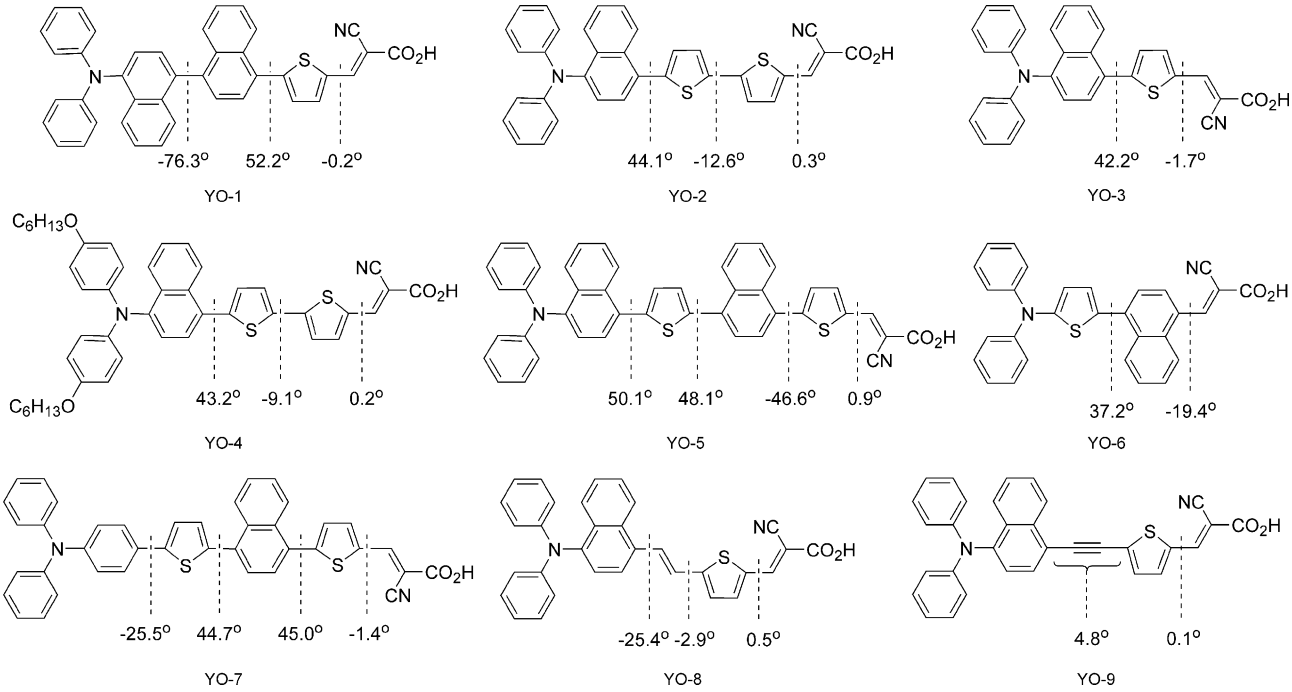

Scheme 4. Structures and dihedral angles of all compounds.

be a result of the lower dye density on TiO_2 and lower molar extinction coefficient.

The dihedral angles between successive units of the molecules are shown in Scheme 4. It is noteworthy that the optimized geometry of the molecule YO-8 is in agreement with the molecular structure obtained from single-crystal X-ray diffraction analysis (Figure S1 in the Supporting Information), confirming the validity of the computation. The dihedral angle (>40°) between the naphthyl entity and the neighboring aromatic ring is large in all compounds, and it even reaches about 75° between the two naphthyl units of YO-1. In accordance with the electronic spectra and cell performances, large dihedral angles in these compounds hamper coplanarity of the spacers and efficient charge transfer from the donor to the acceptor. To facilitate formation of the quinoid structure from the naphthyl moiety for better light harvesting, incorporation of alkenyl entities on both sides of the naphthyl moiety for alleviation of steric congestion is therefore needed. Compared with the compounds in this study, the dyes with a 2,6-naphthyl entity in the spacer have smaller twist angles.[25] Consequently, the 2,6-naphthyl compounds have more efficient charge transfer, leading to better light harvesting and cell performance, although loss of resonance energy is expected to be more serious for a 2,6-naphthyl entity than for a 1,4-naphthyl entity in forming the quinoid structure during the charge-transfer transition.

Conclusion

We synthesized a series of dyes containing a naphthyl-based conjugated spacer between an arylamine donor and a 2-cyanoacrylic acid acceptor. Significant deviation of the naphthyl unit from coplanarity with the neighboring aromatic rings hampered formation of the quinoid structure by the naphthyl unit. The performance of DSSCs with these dyes as the sensitizers exhibited efficiencies ranging from 2.76 to 4.55% under illumination from one sun (AM 1.5). The best performance of the device was achieved with the use of a dye containing an alkenyl unit between the naphthyl and aromatic moieties, and the cell efficiency reached 62% of that of an N719-based DSSC (7.31%) fabricated and measured under similar conditions. Alleviation of steric congestion upon insertion of the alkenyl unit apparently results in longer wavelength absorption of the dye and increases the overall power efficiency of DSSCs.

Experimental Section

General Information

^1H and ^{13}C NMR spectra were recorded on Bruker AMX-400 or Bruker AV-400 spectrometers by using $CDCl_3$, [D_6]acetone, [D_6]dimethylsulfoxide (DMSO), or [D_8]THF as the solvent. CV measurements were performed on a BAS-100 instrument by using CH_2Cl_2 as solvent. UV/Vis spectra were recorded on a Varian Cary 50 spectrophotometer. PL spectra were recorded on a Hitachi F-4500 spectrophotometer. Elemental analysis was performed on a Perkin–Elmer 2400 instrument. Fast-atom bombardment mass spectrometry (FABMS) analysis was performed on a JEOL Tokyo Japan JMS-700 mass spectrometer equipped

with a standard FAB source. The photoelectrochemical characterizations on the solar cells were carried out by using an Oriel Class A solar simulator (Oriel 91195A, Newport Corp.). Photocurrent–voltage characteristics of the DSSCs were recorded with a potentiostat/galvanostat (CHI650B, CH Instruments, Inc.) at a light intensity of 100 mW cm^{-2} calibrated by an Oriel reference solar cell (Oriel 91150, Newport Corp.). The monochromatic quantum efficiency was recorded through a monochromator (Oriel 74100, Newport Corp.) under short-circuit conditions. The intensity of each wavelength was in the range of 1–3 m W cm^{-2}. Electrochemical impedance spectra were recorded for DSSCs under illumination at an open-circuit voltage (V_{OC}) or dark at a potential of −0.55 V at room temperature. The frequencies explored ranged from 10 mHz to 100 kHz. The TiO_2 nanoparticles and the reference compound, N719, were purchased from Solaronix, S.A., Switzerland.

Devices Fabrication

The photoanode used was a TiO_2 thin film (12 μm of 20 nm particles as the absorbing layer and 6 μm of 400 nm particles as the scattering layer) coated on an FTO glass substrate with dimensions of 0.5×0.5 cm^2.[26] The film thickness was measured by a profilometer (Dektak3, Veeco/Sloan Instruments Inc., USA). Platinized FTO produced by thermopyrolysis of H_2PtCl_6 was used as a counter electrode. The TiO_2 thin film was dipped into a 3×10^{-4} M solution of the dye sensitizers in THF for at least 12 h. After rinsing with THF, the photoanode adhered to a polyester tape 60 μm thick with a square aperture of 0.36 cm^2 was placed on top of the counter electrode and tightly clipped together to form the cell. Electrolyte was then injected into the space and then the cell was sealed with Torr Seal cement (Varian, MA, USA). The electrolyte was composed of 0.5 M LiI, 0.05 M I_2, and 0.5 M TBP that was dissolved in acetonitrile.

Quantum Chemistry Calculations

Calculations were performed with Q-Chem 3.0 software.[27] Geometry optimization of the molecules were performed by using a hybrid B3LYP functional and 6-31G* basis set. For each molecule, a number of possible conformations were examined and the one with the lowest energy was used. The same functional was also applied for the calculation of excited states by TD-DFT. A number of previous works employed TD-DFT to characterize excited states with charge-transfer character.[28] In some cases, underestimation of the excitation energies was seen.[27,29] Therefore, in the present work, we used TD-DFT to visualize the extent of transition moments as well as their charge-transfer characters, and avoided drawing conclusions from the excitation energy.

Synthesis

Compounds YO-2 to YO-9 were synthesized from appropriate aldehydes in the same manner as that of YO-1. Details of intermediates are described in the Supporting Information.

Compound YO-1

Precursor **4** (0.80 g, 1.5 mmol), NH_4OAc (0.03 g, 0.3 mol%), and 2-cyanoacetic acid (0.17 g, 2.0 mmol) were dissolved in acetic acid (10 mL) in a 100 mL round-bottomed flask. The resulting solution was heated to reflux for 10 h. The solution was extracted with dichloromethane and water, and the organic extracts collected were dried over $MgSO_4$. The crude product was further purified by column chromatography on silica gel by eluting with CH_2Cl_2/MeOH (20:1 by v/v) to give YO-1 (80%, 0.72 g). ^{1}H NMR (400 MHz, [D$_6$]acetone): δ = 8.55 (s, 1H), 8.37 (d, J = 8.0 Hz, 1H), 8.36–8.11 (m, 2H), 7.89 (d, J = 7.2 Hz, 1H), 7.70–7.62 (m, 4H), 7.56–7.35 (m, 6H), 7.30 (t, J = 8.0 Hz, 4H), 7.12 (d, J = 8.0 Hz, 4H), 7.01 ppm (t, J = 8.0 Hz, 1H); MS (FAB): m/z: 598.2 [M^+]; elemental analysis calcd (%) for $C_{40}H_{26}N_2O_2S$: C 80.24, H 4.38, N 4.68; found: C 80.22, H 4.66, N 5.00.

Compound YO-2

Yield: 82%; ^{1}H NMR (400 MHz, [D$_6$]acetone): δ = 8.42 (s, 1H), 8.37 (d, J = 8.4 Hz, 1H), 8.08 (d, J = 8.4 Hz, 1H), 7.94 (d, J = 4.0 Hz, 1H), 7.74 (d, J = 8.0 Hz, 1H), 7.71 (d, J = 4.0 Hz, 1H), 7.60 (t, J = 8.4 Hz, 1H), 7.58 (d, J = 4.0 Hz, 1H), 7.48 (t, J = 7.6 Hz, 1H), 7.43 (d, J = 4.0 Hz, 1H), 7.40 (d, J = 8.0 Hz, 1H), 7.27 (t, J = 8.0 Hz, 4H), 7.04 (d, J = 8.0 Hz, 4H), 7.00 ppm (d, J = 8.0 Hz, 2H); ^{13}C NMR ([D$_6$]DMSO, 125 MHz): δ = 163.5, 147.7, 146.3, 145.3, 143.8, 142.6, 141.3, 135.3, 134.1, 132.3, 130.8, 129.6, 129.4, 128.9, 128.8, 127.5, 127.3, 126.9, 126.5, 125.7, 125.2, 124.2, 122.1, 121.6, 116.4, 98.2 ppm; MS (FAB): m/z: 554.1 [M^+]; elemental analysis calcd (%) for $C_{34}H_{22}N_2O_2S_2$: C 73.62, H 4.00, N 5.05; found: C 73.22, H 4.19, N 5.19.

Compound YO-3

Yield: 52%; ^{1}H NMR (400 MHz, $CDCl_3$): δ = 8.39 (s, 1H), 8.16 (d, J = 8.4 Hz, 1H), 8.02 (d, J = 8.4 Hz, 1H), 7.91 (d, J = 4.0 Hz, 1H), 7.58 (d, J = 8.0 Hz, 1H), 7.49 (t, J = 7.6 Hz, 1H), 7.41 (d, J = 4.0 Hz, 1H), 7.38 (t, J = 7.6 Hz, 1H), 7.31 (d, J = 8.0 Hz, 1H), 7.21 (t, J = 7.6 Hz, 4H), 7.03 (d, J = 7.6 Hz, 4H), 6.96 ppm (t, J = 7.6 Hz, 2H); ^{13}C NMR ([D$_8$]THF, 100 MHz): δ = 164.1, 152.3, 149.7, 146.8, 146.6, 145.4, 138.9, 137.6, 134.2, 132.5, 130.1, 130.0, 129.7, 127.7, 127.6, 127.4, 127.3, 126.8, 126.0, 122.9, 116.6, 100.9 ppm; MS (FAB): m/z: 472.1 [M^+]; elemental analysis calcd (%) for $C_{30}H_{20}N_2O_2S$: C 76.25, H 4.27, N 5.93; found: C 75.92, H 4.55, N 6.04.

Compound YO-4

Yield: 46%; ^{1}H NMR (400 MHz, [D$_6$]acetone): δ = 8.47 (s, 1H), 8.33 (d, J = 8.4 Hz, 1H), 8.12 (d, J = 8.4 Hz, 1H), 7.99 (d, J = 4.0 Hz, 1H), 7.73 (d, J = 4.0 Hz, 1H), 7.67 (d, J = 8.0 Hz, 1H), 7.60–7.55 (m, 2H), 7.44 (t, J = 8.0 Hz, 1H), 7.25 (d, J = 8.0 Hz, 1H), 6.92 (d, J = 8.0 Hz, 4H), 6.84 (d, J = 8.0 Hz, 4H), 3.95 (t, J = 6.6 Hz, 4H), 1.80–1.71 (m, 4H), 1.48–1.45 (m, 4H), 1.35–1.34 (m, 8H), 0.92–0.88 ppm (m, 6H); ^{13}C NMR ([D$_8$]THF, 125 MHz): δ = 164.1, 156.0, 147.3, 147.2, 146.5, 145.2, 143.8, 140.2, 137.0, 135.9, 134.3, 132.0, 130.0, 129.6, 129.2, 127.8, 127.6, 126.9, 126.8, 126.3, 125.6, 125.5, 125.0, 116.7, 116.0, 100.0, 68.9, 68.1, 32.8, 30.5, 26.9, 26.5, 25.0, 23.7, 14.5 ppm; MS (FAB): m/z: 754.3 [M^+]; elemental analysis calcd (%) for $C_{46}H_{46}N_2O_4S_2$: C 73.18, H 6.14, N 3.71; found: C 73.37, H 6.45, N 3.90.

Compound YO-5

Yield: 20%; ^{1}H NMR (400 MHz, [D$_6$]acetone): δ = 8.57 (s, 1H), 8.56–8.55 (m, 1H), 8.48 (d, J = 8.4 Hz, 1H), 8.36–8.33 (m, 1H), 8.16 (d, J = 4.0 Hz, 1H), 8.10 (d, J = 8.4 Hz, 1H), 7.85–7.78 (m, 3H), 7.74–7.71 (m, 2H), 7.64–7.60 (m, 2H), 7.55–7.49 (m, 3H), 7.43 (d, J = 7.6 Hz, 1H), 7.29–7.24 (m, 4H), 7.06–7.04 (m, 4H), 7.01–6.98 ppm (m, 2H); ^{13}C NMR ([D$_8$]THF, 125 MHz): δ = 149.7, 146.9, 145.4, 143.7, 139.1, 132.5, 130.3, 130.1, 129.8, 129.4, 129.2, 129.0, 128.5, 128.2, 128.0, 127.7, 127.5, 127.4, 127.3, 126.7, 123.2, 123.0, 119.3, 116.7, 101.0 ppm; MS (FAB): m/z: 681.2 [M^+]; elemental analysis calcd (%) for $C_{44}H_{28}N_2O_2S_2$: C 77.62, H 4.15, N 4.11; found: C 77.38, H 4.17, N 4.60.

Compound YO-6

Yield: 44%; ^{1}H NMR (400 MHz, [D$_6$]acetone): δ = 9.13 (s, 1H), 8.54 (d, J = 8.0 Hz, 1H), 8.29 (d, J = 7.6 Hz, 1H), 8.21 (d, J = 8.0 Hz, 1H), 7.78–7.70 (m, 3H), 7.40–7.36 (d, J = 7.6 Hz, 4H), 7.28 (d, J = 4.0 Hz, 1H), 7.25 (d, J = 7.6 Hz, 4H), 7.12 (t, J = 7.6 Hz, 2H), 6.86 ppm (d, J = 4.0 Hz, 1H); ^{13}C NMR ([D$_8$]THF, 100 MHz): δ = 163.9, 154.5, 152.2, 149.0, 138.5, 135.2, 133.6, 133.5, 132.5, 130.3, 129.5, 128.6, 128.5, 128.4, 128.1, 128.0, 127.7, 124.6, 124.4, 124.2, 124.0, 123.9, 123.7, 121.6, 116.1, 108.1 ppm; MS (FAB): m/z: 473.1 [M^+]; elemental analysis calcd (%) for $C_{30}H_{20}N_2O_2S$: C 76.25, H 4.27, N 5.93; found: C 75.88, H 4.52, N 5.65.

Compound YO-7

Yield: 77%; ^{1}H NMR (400 MHz, [D$_6$]acetone): δ = 8.57 (s, 1H), 8.49–8.47 (m, 1H), 8.33–8.31 (m, 1H), 8.15 (d, J = 4.0 Hz, 1H), 7.80–7.76 (m, 2H), 7.71–7.67 (m, 4H), 7.62 (d, J = 4.0 Hz, 1H), 7.54 (d, J = 4.0 Hz, 1H), 7.38 (d, J = 3.6 Hz, 1H), 7.35 (t, J = 8.0 Hz, 4H), 7.14–7.08 ppm (m, 8H); ^{13}C NMR (100 MHz, [D$_8$]THF): δ = 164.3, 152.2, 148.7, 146.8, 146.2, 140.7, 139.0, 137.8, 135.2, 133.3, 132.9, 132.2, 130.3, 130.1, 129.4, 128.9, 128.3, 128.2, 127.9, 127.5, 127.4, 126.6, 125.6, 124.6, 124.2, 123.9, 116.7, 101.0 ppm; MS (FAB): m/z: 631.1 [M^+]; elemental analysis calcd (%) for $C_{40}H_{26}N_2O_2S_2$: C 76.16, H 4.15, N 4.44; found: C 75.92, H 4.45, N 4.37.

Compound YO-8

Yield: 55%; ^{1}H NMR (400 MHz, [D$_6$]DMSO): δ=8.47 (s, 1H), 8.43 (d, J=8.5, 1H), 8.09–8.13 (m, 1H), 7.97–8.40 (m, 2H), 7.91 (d, J=8.3, 1H), 7.59–7.69 (m, 3H), 7.47 (t, J=7.5, 1H), 7.34 (d, J=7.7, 1H), 7.24 (t, J=7.5, 4H), 6.90–7.00 ppm (m, 6H); ^{13}C NMR ($CDCl_3$, 125 MHz): 206.5, 163.7, 151.8, 147.8, 146.3, 143.8, 141.0, 134.5, 132.4, 131.4, 130.6, 129.4, 128.4, 127.4, 126.9, 126.8, 126.7, 124.7, 124.4, 124.2, 123.4, 122.1, 121.6, 116.6, 98.3, 30.7 ppm; MS (FAB): m/z: 498 [M^+]; elemental analysis calcd (%) for $C_{32}H_{22}N_2O_2S$ (YO-8·C_3H_6O): C 75.52, H 5.07, N 5.03; found: C 75.52, H 5.06, N 5.66. The compound was recrystallized from acetone and diethyl ether, and one equivalent of acetone was found to cocrystallize with the compound.

Compound YO-9

Yield: 90%; ^{1}H NMR (400 MHz, [D$_6$]DMSO): δ=8.32 (d, J=8.4 Hz, 1H), 7.93 (d, J=8.5 Hz, 1H), 7.69–7.73 (m, 2H), 7.53–7.59 (m, 1H), 7.32–7.39 (m, 2H), 7.13–7.30 (m, 6H), 6.92–7.13 ppm (m, 6H); ^{13}C NMR (100 MHz, $CDCl_3$): δ=87.5, 97.8, 117.3, 122.6, 122.8, 125.1, 126.1, 126.7, 127.1, 127.6, 129.4, 130.7, 131.8, 132.7, 133.0, 134.9, 137.1, 138.2, 145.9, 148.5, 182.5 ppm; MS (FAB): m/z: 496 [M^+]; HRMS: m/z calcd for $C_{32}H_{20}N_2O_2S$: 496.1245; found: 496.1245; elemental analysis calcd (%) for $C_{32}H_{22}N_2O_2S$: C 77.40, H 4.06, N 5.64; found: C 77.90, H 4.28, N 5.59.

Crystal Structure Analysis

An orange prism-like specimen (dimensions $0.18\times0.1\times0.08$ mm^3) obtained by slow diffusion of Et_2O into a solution of the compound in acetone was used for the X-ray crystallographic analysis. The single-crystal X-ray diffraction experiments were carried out at 100.0(1) K by using graphite-monochromated $Mo_{K\alpha}$ radiation (λ=0.71073 Å) on a Bruker SMART CCD diffractometer. A total of 676 frames were collected. The frames were integrated with the CrysAlisPro, Oxford Diffraction, Version 1.171.34.40 (released 27-08-2010 CrysAlis171 NET; compiled Aug 27 2010, 11:50:40) software package using a narrow-frame algorithm. Integration of the data using a triclinic unit cell yielded a total of 24934 reflections to a maximum θ angle of 29.48° (0.80 Å resolution), of which 6903 were independent and 4587 (99.8%) were greater than $2\sigma(F^2)$. Final cell constants of a=9.2816(5), b=9.3435(4), c=17.8317(9) Å; α=97.474(4), β=98.226(4), γ=113.725(4)°; and V=1370.78(12) Å^3 are based upon the refinement of 5411 reflections with $5.74°<2\theta<58.97°$. Data were corrected for absorption effects by using the multiscan method. The ratio of minimum to maximum apparent transmission was 0.993. The calculated minimum and maximum transmission coefficients (based on crystal size) were 0.9927 and 1.0000. The structure was solved and refined by using the SHELXS-97 (Sheldrick, 1997) software package, using the space group $P-1$, with Z=2 for the formula unit $C_{35}H_{28}N_2O_3S$. The final anisotropic full-matrix least-squares refinement on F^2 with 377 variables converged at $R1$=5.58%, for the observed data and $wR2$=11.74% for all data. The goodness-of-fit was 1.064. The largest peak in the final difference electron density synthesis was 0.739 e$^-$ Å^3 and the largest hole was −0.3868 e$^-$ Å^3 with a root-mean-square (RMS) deviation of 0.067 e$^-$ Å^3. On the basis of the final model, the calculated density was 1.349 g cm^{-3} and F(000) was 584 e$^-$. The compound crystallized with one molecule of acetone. Crystal data and structure refinement parameters are given in the Supporting Information.

CCDC 856091 contains the supplementary crystallographic data for this paper. These data can be obtained free of charge from The Cambridge Crystallographic Data Centre via www.ccdc.cam.ac.uk/data_request/cif.

Acknowledgements

We acknowledge the support of the Academia Sinica (A.C.) and NSC (Taiwan), and the Instrumental Center of Institute of Chemistry (A.C.).

[1] B. O'Regan, M. Grätzel, *Nature* **1991**, *353*, 737–740.
[2] A. Hagfeldt, G. Boschloo, L. Sun, L. Kloo, H. Pettersson, *Chem. Rev.* **2010**, *110*, 6595–6663.
[3] Y. Ooyama, Y. Harima, *Eur. J. Org. Chem.* **2009**, 2903–2934.
[4] a) M. Grätzel, *Inorg. Chem.* **2005**, *44*, 6841–6851; b) Y. Cao, Y. Bai, Q. Yu, Y. Cheng, S. Liu, D. Shi, F. Gao, P. Wang, *J. Phys. Chem. C* **2009**, *113*, 6290–6297; c) C. Y. Chen, M. Wang, J. Y. Li, N. Pootrakulchote, L. Alibabaei, C. Ngoc-le, J. D. Decoppet, J. H. Tsai, C. Grätzel, C. G. Wu, S. M. Zakeeruddin, M. Grätzel, *ACS Nano* **2009**, *3*, 3103–3109.
[5] a) A. Mishra, M. K. R. Fischer, P. Bauerle, *Angew. Chem.* **2009**, *121*, 2510–2536; *Angew. Chem. Int. Ed.* **2009**, *48*, 2474–2499; b) B. S. Chen, D. Y. Chen, C. L. Chen, C. W. Hsu, H. C. Hsu, K. L. Wu, S. H. Liu, P. T. Chou, Y. Chi, *J. Mater. Chem.* **2011**, *21*, 1937–1945; c) D. Zhou, N. Cai, H. Long, M. Zhang, Y. Wang, P. Wang, *J. Phys. Chem. C* **2011**, *115*, 3163–3171; d) W. Zhu, Y. Wu, S. Wang, W. Li, X. Li, J. Chen, Z. S. Wang, H. Tian, *Adv. Funct. Mater.* **2011**, *21*, 756–763; e) Z. Ning. Y. Fu, H. Tian, *Energy Environ. Sci.* **2010**, *3*, 1170–1181; f) Z. Ning, Q. Zhang, H. Pei, J. Luan, C. Lu, Y. Cui, H. Tian, *J. Phys. Chem. C* **2009**, *113*, 10307–10313.
[6] W. Zeng, Y. Cao, Y. Bai, Y. Wang, Y. Shi, M. Zhang, F. Wang, C. Pan, P. Wang, *Chem. Mater.* **2010**, *22*, 1915–1925.
[7] G. Zhang, H. Bala, Y. Cheng, D. Shi, X. Lv, Q. Yu, P. Wang, *Chem. Commun.* **2009**, 2198–2200.
[8] a) C. H. Chen, Y. C. Hsu, H. H. Chou, K. R. Justin Thomas, J. T. Lin, C. P. Hsu, *Chem. Eur. J.* **2010**, *16*, 3184–3193; b) J. T. Lin, P. C. Chen, Y. S. Yen, Y. C. Hsu, H. H. Chou, M. C. P. Yeh, *Org. Lett.* **2009**, *11*, 97–100; c) Y. S. Yen, Y. C. Hsu, J. T. Lin, C. W. Chang, C. P. Hsu, D. J. Yin, *J. Phys. Chem. C* **2008**, *112*, 12557–12567; d) K. R. Justin Thomas, Y. C. Hsu, J. T. Lin, K. M. Lee, K. C. Ho, C. H. Lai, Y. M. Cheng, P. T. Chou, *Chem. Mater.* **2008**, *20*, 1830–1840.
[9] a) Y. J. Cheng, S. H. Yang, C. S. Hsu, *Chem. Rev.* **2009**, *109*, 5868–5923; b) M Alicia, A. M. Fraind, J. D. Tovar, *J. Phys. Chem. B* **2010**, *114*, 3104–3116.
[10] I. D. L. Albert, J. O. Morley, D. Pugh, *J. Phys. Chem.* **1995**, *99*, 8024–8032.
[11] C. Teng, X. Yang, C. Yang, S. Li, M. Cheng, A. Hagfeldt, L. Sun, *J. Phys. Chem. C* **2010**, *114*, 9101–9110.
[12] M. Tanaka, S. Hayashi, S. Eu, T. Umeyama, Y. Matano, H. Imahori, *Chem. Commun.* **2007**, 2069–2071.
[13] a) J. F. Hartwig, *Angew. Chem.* **1998**, *110*, 2154–2177; *Angew. Chem. Int. Ed.* **1998**, *37*, 2046–2067; b) J. P. Wolfe, S. Wagaw, J.-F. Marcoux, S. L. Buchwald, *Acc. Chem. Res.* **1998**, *31*, 805–818.
[14] J. K. Stille, *Angew. Chem.* **1986**, *98*, 504–519; *Angew. Chem. Int. Ed. Engl.* **1986**, *25*, 508–524.
[15] K. Sonogashira, Y. Tohda, N. Hagihara, *Tetrahedron Lett.* **1975**, *16*, 4467–4470.
[16] a) N. S. Baek, J. S. Yum, H. K. Kim, M. K. Nazeeruddin, M. Grätzel, *Energy Environ. Sci.* **2009**, *2*, 1082–1087; b) A. Bhaskar, G. Ramakrishna, Z. Lu, R. Twieg, J. M. Hales, T. Goodson III., *J. Am. Chem. Soc.* **2006**, *128*, 11840–11849; c) D. H. Lee, M. J. Lee, H. M. Song, B. J. Song, K. D. Seo, M. Pastore, C. Anselmi, S. Fantacci, F. De Angelis, M. K. Nazeeruddin, M. Grätzel, H. K. Kim, *Dyes Pigm.* **2011**, *91*, 192–198.
[17] D. P. Hagberg, T. Marinado, K. M. Karlsson, K. Nonomura, P. Qin, G. Boschloo, T. Brinck, A. Hagfeldt, L. Sun, *J. Org. Chem.* **2007**, *72*, 9550–9556.
[18] a) K. Hara, T. Sato, R. Katoh, A. Furube, Y. Ohga, A. Shinpo, S. Suga, K. Sayama, H. Sugihara, H. Arakawa, *J. Phys. Chem. B* **2003**, *107*, 597–606; b) K. Hara, Y. Tchibana, Y. Ohga, A. Shinpo, S. Suga, K. Sayama, H. Sugihara, H. Arakawa, *Sol. Energy Mater. Sol. Cells* **2003**, *77*, 89–103; c) S.-L. Li, K.-J. Jiang, K.-F. Shao, L.-M. Yang, *Chem. Commun.* **2006**, 2792–2794.
[19] M. Velusamy, Y. C. Hsu, J. T. Lin, C. W. Chang, C. P. Hsu, *Chem. Asian J.* **2010**, *5*, 87–96.
[20] a) S.-J. Moon, J.-H. Yum, R. Humphry-Baker, K. M. Karlsson, D. P. Hagberg, T. Marinado, A. Hagfeldt, L. Sun, M. Grätzel, M. K. Nazeeruddin, *J. Phys. Chem. C* **2009**, *113*, 16816–16820; b) L.-Y. Lin,

C.-H. Tsai, K.-T. Wong, T.-W. Huang, C.-C. Wu, S.-H. Chou, F. Lin, S.-H. Chen, A.-I. Tsai, *J. Mater. Chem.* **2011**, *21*, 5950–5958.
[21] M. Velusamy, K. R. Justin Thomas, J. T. Lin, Y.-C. Hsu, K.-C. Ho, *Org. Lett.* **2005**, *7*, 1899–1902.
[22] J. He, W. Wu, J. Hua, Y. Jiang, S. Qu, J. Li, Y. Long, H. Tian, *J. Mater. Chem.* **2011**, *21*, 6054–6062.
[23] A. Hagfeldt, M. Grätzel, *Chem. Rev.* **1995**, *95*, 49–68.
[24] a) Q. Wang, J. E. Moser, M. Grätzel, *J. Phys. Chem. B* **2005**, *109*, 14945–14953; b) M. Adachi, M. Sakamoto, J. Jiu, Y. Ogata, S. Isoda, *J. Phys. Chem. B* **2006**, *110*, 13872–13880.
[25] C. Olivier, F. Sauvage, L. Ducasse, F. Castet, M. Grätzel, T. Toupance, *ChemSusChem* **2011**, *4*, 731–736.
[26] Y. S. Yen, Y. C. Chen, Y. C. Hsu, H. H. Chou, J. T. Lin, D. J. Yin, *Chem. Eur. J.* **2011**, *17*, 6781–6788.
[27] Y. Shao, L. F. Molnar, Y. Jung, J. Kussmann, C. Ochsenfeld, S. T. Brown, A. T. B. Gilbert, L. V. Slipchenko, S. V. Levchenko, D. P. O'Neill, R. A. DiStasio, Jr., R. C. Lochan, T. Wang, G. J. O. Beran, N. A. Besley, J. M. Herbert, C. Y. Lin, T. V. Voorhis, S. H. Chien, A. Sodt, R. P. Steele, V. A. Rassolov, P. E. Maslen, P. P. Korambath, R. D. Adamson, B. Austin, J. Baker, E. F. C. Byrd, H. Dachsel, R. J. Doerksen, A. Dreuw, B. D. Dunietz, A. D. Dutoi, T. R. Furlani, S. R. Gwaltney, A. Heyden, S. Hirata, C.-P. Hsu, G. Kedziora, R. Z. Khalliulin, P. Klunzinger, A. M. Lee, M. S. Lee, W. Z. Liang, I. Lotan, N. Nair, B. Peters, E. I. Proynov, P. A. Pieniazek, Y. M. Rhee, J. Ritchie, E. Rosta, C. D. Sherrill, A. C. Simmonett, J. E. Subotnik, H. L. Woodcock III, W. Zhang, A. T. Bell, A. K. Chakraborty, *Phys. Chem. Chem. Phys.* **2006**, *8*, 3172–3191.
[28] a) H. M. Vaswani, C. P. Hsu, M. Head-Gordon, G. R. Fleming, *J. Phys. Chem. B* **2003**, *107*, 7940–7946; b) Y. Kurashige, T. Nakajima, S. Kurashige, K. Hirao, Y. Nishikitani, *J. Phys. Chem. A* **2007**, *111*, 5544–5548.
[29] A. Dreuw, M. Head-Gordon, *J. Am. Chem. Soc.* **2004**, *126*, 4007–4016.

Received: November 30, 2011
Published online: March 1, 2012

